Vasken Dilsizian
Jagat Narula
Editors

Atlas of Nuclear Cardiology

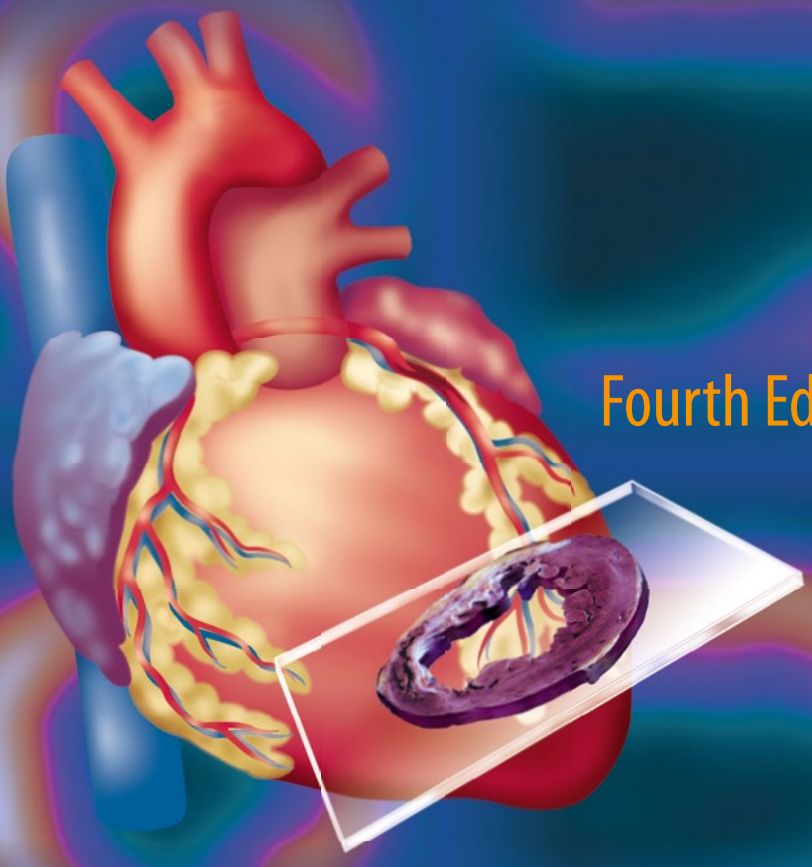

Fourth Edition

Springer

Atlas of Nuclear Cardiology

Vasken Dilsizian • Jagat Narula
Editors

Atlas of Nuclear Cardiology

Fourth Edition

Springer

Editors
Vasken Dilsizian, M.D.
Professor of Medicine and Radiology
University of Maryland School of Medicine
Chief, Division of Nuclear Medicine
University of Maryland Medical Center
Baltimore
Maryland
USA

Jagat Narula, M.D., Ph.D.
Philip J. and Harriet L.
Goodhart Chair in Cardiology
Professor of Medicine
Associate Dean for Global Health
Director, Cardiovascular Imaging Program
Zena and Michael A. Wiener
Cardiovascular Institute
Mount Sinai School of Medicine
New York
NY
USA

ISBN 978-1-4614-5549-3 ISBN 978-1-4614-5551-6 (eBook)
DOI 10.1007/978-1-4614-5551-6
Springer New York Heidelberg Dordrecht London

Library of Congress Control Number: 2012953563

Printed on acid-free paper

Springer is part of Springer Science+Business Media (www.springer.com)

Preface

Over the past three decades, nuclear cardiology has evolved from a research tool into a well-established clinical discipline. Approximately nine million nuclear cardiology procedures are performed annually in the United States. The field has excelled in the noninvasive evaluation and quantification of myocardial perfusion, function, metabolism, and innervation. Unlike anatomically oriented approaches to diagnostic medicine, the strengths of nuclear techniques are based on physiologic, biochemical, and molecular properties. The ability to define myocardial perfusion, viability, and ventricular function from a single study has become a powerful diagnostic and prognostic tool. As a result of its important contribution to the management and care of cardiac patients, nuclear cardiology is now recognized as a distinct clinical entity.

Nuclear cardiology first originated as a discipline in the early 1970s. A major breakthrough in the field came with the development of myocardial perfusion radiotracers, such as ^{201}TI, which permitted noninvasive detection and physiologic characterization of anatomic coronary artery lesions. First-pass and equilibrium radionuclide angiography allowed for the noninvasive assessment of regional and global left ventricular function. The field blossomed further with incorporation of the concepts of exercise physiology, demand-supply mismatch, coronary vasodilator reserve, and systolic and diastolic left ventricular dysfunction in nuclear testing. Pharmacologic vasodilators, such as dipyridamole, adenosine, and the more recent introduction of the selective A_{2A} receptor agonist regadenoson, widened the application of myocardial perfusion studies to patients who were unable to exercise, had uncomplicated acute coronary syndromes, or were undergoing intermediate- to high-risk noncardiac surgical procedures. Subsequently, the field advances from detection of coronary artery disease to risk stratification and prognosis. As such, nuclear cardiology procedures have become the cornerstone of the decision-making process to appropriately select patients for medical or interventional therapy, as well as monitoring the effectiveness of that therapy.

Parallel advances in both radiopharmaceuticals and instrumentation have further fostered the growth of nuclear cardiology. The introduction of ^{99m}Tc-labeled perfusion tracers in the 1990s improved the count rate and image quality of myocardial perfusion studies, which allowed for electrocardiogram-gated acquisition and simultaneous assessment of regional myocardial perfusion and function with a single radiotracer. Because ^{99m}Tc-labeled perfusion tracers demonstrate minimal redistribution over time after injection, they have been used in the emergency room and in the early hours of an infarct to estimate the extent of myocardium in jeopardy. A follow-up study, performed several days later, provides information on final infarct size and myocardial salvage. PET has broadened the scope of the cardiac examination from perfusion and function alone to assessment of metabolic substrate utilization, cardiac receptor occupancy, and adrenergic neuronal function. By allowing the quantification of blood flow in absolute terms, PET has led to a better understanding of the physiologic mechanisms underlying cardiovascular diseases beyond discrete epicardial coronary artery disease, such as coronary vasomotor function in the early stages of coronary atherosclerosis development, hypertrophic cardiomyopathy, and dilated nonischemic cardiomyopathy. The ability to image the shift in the primary source of myocardial energy production from fatty acids toward glucose utilization in the setting of reduced blood flow has helped explain the pathophysiology of

hibernation and myocardial viability, as well as management of patients with chronic ischemic left ventricular dysfunction and heart failure for the assessment of myocardial viability. Targeted molecular imaging and image-guided therapy will further improve the management of heart disease by identifying patients for whom the response to medical therapy would be optimal, or perhaps not beneficial at all, as we move closer to personalized medicine.

The aim of the fourth edition of the *Atlas of Nuclear Cardiology* is to elucidate the role of cardiovascular nuclear procedures in the clinical practice of cardiology. Diagnostic algorithms and schematic diagrams integrated with nuclear cardiology procedures are generously interspersed with color illustrations to emphasize key concepts in cardiovascular physiology, pathology, metabolism, and innervation. In the first chapter, the principles of nuclear cardiology imaging along with an introduction to instrumentation and image acquisition are presented. The next three chapters (Chaps. 2, 3, and 4) detail SPECT and PET radiopharmaceuticals, hybrid SPECT/CT and PET/CT imaging techniques, and physiologic and pharmacologic stressors for the detection of coronary artery disease. In Chap. 5, the potential benefits of quantitative approaches that measure myocardial blood flow and its changes in response to interventions are presented in absolute and relative terms. In Chap. 6, the techniques of first-pass and equilibrium radionuclide angiography and gated myocardial perfusion SPECT are reviewed for assessment of cardiac function. Chapter 7 details current evidence for the use of myocardial perfusion imaging for risk stratification in patients with chronic coronary artery disease; in special populations such as women, diabetics, the elderly, and patients of diverse ethnicity; and for identifying survival benefits with revascularization versus medical therapy. The next two chapters (Chaps. 8 and 9) focus on the role of imaging cardiac metabolism in identifying ischemic and viable myocardium as well as new neurohumoral targets for prevention of heart failure and left ventricular remodeling. Chapter 10 addresses the role of cardiac imaging in the diagnosis and risk stratification of patients suffering from acute coronary syndromes. The last two chapters (Chaps. 11 and 12) examine the latest approaches of radionuclide techniques for the advancement of cardiovascular research: myocardial innervation and molecular imaging of atherosclerosis.

In the next century, innovative imaging strategies in nuclear cardiology will propel the field into molecular imaging and personalized medicine while it continues to build on its already well-defined strengths of myocardial perfusion, function, and metabolism. Realization of these ideas and progress in the diagnosis, treatment, and prevention of cardiovascular disease will depend not only on new discoveries but also on meaningful interaction between clinicians and investigators. It is our hope that the fourth edition of the *Atlas of Nuclear Cardiology* will serve as a foundation for clinicians and a reference guide for scientists within and outside the field.

Vasken Dilsizian
Jagat Narula

Contents

Contributors

Stephen L. Bacharach, Ph.D. Department of Radiology, University of California, San Francisco, San Francisco, CA, USA

Frank M. Bengel, M.D. Department of Nuclear Medicine, Hannover Medical School, Hannover, Germany

Daniel Berman, M.D. Nuclear Cardiology/Cardiac Imaging, David Geffen School of Medicine at UCLA and Cedars-Sinai Medical Center, Los Angeles, CA, USA

Elias H. Botvinick, M.D. Department of Radiology and Biomedical Imaging, University of California, San Francisco, San Francisco, CA, USA

Ji Chen, Ph.D. Department of Radiology, Emory University School of Medicine, Atlanta, GA, USA

Nick G. Costouros, M.D. Department of Radiology and Nuclear Medicine, Palo Alto Medical Foundation, Palo Alto, CA, USA

Vasken Dilsizian, M.D. Professor of Medicine and Radiology, University of Maryland School of Medicine Chief, Division of Nuclear Medicine University of Maryland Medical Center, Baltimore, Maryland, USA

Tracy L. Faber, Ph.D. Department of Radiology, Emory University School of Medicine, Atlanta, GA, USA

James R. Galt, Ph.D. Department of Radiology and Imaging Sciences, Emory University School of Medicine, Atlanta, GA, USA

Ernest V. Garcia, Ph.D. Department of Radiology and Imaging Sciences, Emory University Hospital, Atlanta, GA, USA

Guido Germano, Ph.D., M.B.A. Department of Medicine, Cedars-Sinai Medical Center, Los Angeles, CA, USA

Rory Hachamovitch, M.D., M.Sc. Department of Cardiovascular Medicine, Cleveland Clinic, Cleveland, OH, USA

Farouc A. Jaffer, M.D., Ph.D. Department of Medicine, Harvard Medical School, Boston, MA, USA

Cardiology Division, Department of Medicine, Massachusetts General Hospital, Boston, MA, USA

Juhani Knuuti, M.D., Ph.D. Turku PET Centre, Turku University Hospital and University of Turku, Turku, Finland

Jennifer H. Mieres, M.D. Department of Cardiology, Hofstra North Shore–Long Island Jewish School of Medicine, Lake Success, NY, USA

D. Douglas Miller, M.D., CM, FRCPC, FACP, FACC, FAHA Faculty of Medicine & Dentistry, Department of Medicine (Cardiology), University of Alberta, Edmonton, AB, Canada

Jagat Narula, M.D., Ph.D. Philip J. and Harriet L. Goodhart Chair in Cardiology, Professor of Medicine Associate Dean for Global Health Director, Cardiovascular Imaging Program Zena and Michael A. Wiener Cardiovascular Institute Mount Sinai School of Medicine, New York, NY, USA

J. William O'Connell, M.S. (Retired at) University of California, San Francisco, San Francisco, CA, USA

Antti Saraste, M.D., Ph.D. Turku PET Centre, Turku University Hospital, Turku, Finland

Heinrich R. Schelbert, M.D., Ph.D. Department of Molecular and Medical Pharmacology, David Geffen School of Medicine, University of California, Los Angeles, Los Angeles, CA, USA

Thomas H. Schindler, M.D. Division of Cardiology, Department of Specialties in Medicine, University Hospitals of Geneva, Geneva, Switzerland

Markus Schwaiger, M.D. Department of Nuclear Medicine, Technical University of Munich, Munich, Germany

Leslee J. Shaw, Ph.D. Division of Cardiology, Department of Medicine, Emory University, Atlanta, GA, USA

Chetan Shenoy, M.B.B.S. Division of Cardiology, Department of Medicine, Tufts Medical Center, Boston, MA, USA

Heinrich Taegtmeyer, M.D., D.Phil Division of Cardiology, Department of Internal Medicine, The University of Texas Medical School at Houston, Houston, TX, USA

Ahmed Tawakol, M.D. Cardiology Division, Department of Medicine, Massachusetts General Hospital, Boston, MA, USA

James E. Udelson, M.D. Division of Cardiology, Department of Medicine and Radiology, Tufts Medical Center, Tufts University School of Medicine, Boston, MA, USA

1 Principles of Nuclear Cardiology Imaging

Ernest V. Garcia, James R. Galt, Tracy L. Faber, and Ji Chen

Nuclear cardiology imaging is solidly based on many branches of science and engineering, including nuclear, optical, and mathematical physics; electrical and mechanical engineering; chemistry; and biology. This chapter uses principles from these scientific fields to provide an understanding of both the signals used and the imaging system that captures these signals. These principles have been simplified to fit the scope of this atlas.

Nuclear cardiology's signal is a radioactive tracer, and its imaging systems are either single-photon emission CT or positron emission tomography cameras. This combination has met with remarkable success in clinical cardiology. This success is the result of the combination of sophisticated electronic nuclear instruments and a highly specific signal. The signal is as important as or more important than the imaging system, which can be explained with the following analogy.

When we look at the heavens on a clear night, our naked eye can see stars, objects that are millions of miles away, yet when we look into our patients just a few feet away, even with sophisticated systems, we can sometimes miss a signal associated with cardiac disease. The reason is that a star generates an incredibly powerful signal surrounded by a dark background, a signal much more powerful than the signals we currently use. This analogy provides several lessons. First, it illustrates the need to continue to improve our signals. Second, it provides a motivation: By improving our signal, we have the capacity to detect anything. Finally, it explains the success of nuclear cardiology imaging over cardiovascular MRI, echocardiography, or CT for detecting perfusion abnormalities.

There is a misconception that MRI, echocardiogram, and CT are superior to nuclear cardiology imaging because of their superior spatial resolution. Yet, for detecting perfusion defects, what is really necessary is superior contrast resolution. It is this superior contrast resolution that allows us to differentiate between normal and hypoperfused myocardium, facilitating the visual analysis of nuclear cardiology perfusion images. Because these objects are bright compared with the background, we have been able to develop computer algorithms to totally, automatically, and objectively process and quantify our images, a feat yet to be successfully performed by other modalities.

This chapter explains the many important scientific principles necessary to understand this analogy, as well as nuclear cardiology imaging in general, starting from how radiation is emitted from a nucleus to how these sophisticated imaging systems detect this radiation. These principles are explained at a simple but highly applied level, so the nuclear cardiologist can understand them and apply them in routine clinical practice. The better one's understanding of how images are formed and what can go wrong in their formation, the higher one's accuracy in interpreting studies and the more successful one's practice should be.

V. Dilsizian, J. Narula (eds.), *Atlas of Nuclear Cardiology: Fourth Edition,*
DOI 10.1007/978-1-4614-5551-6_1,

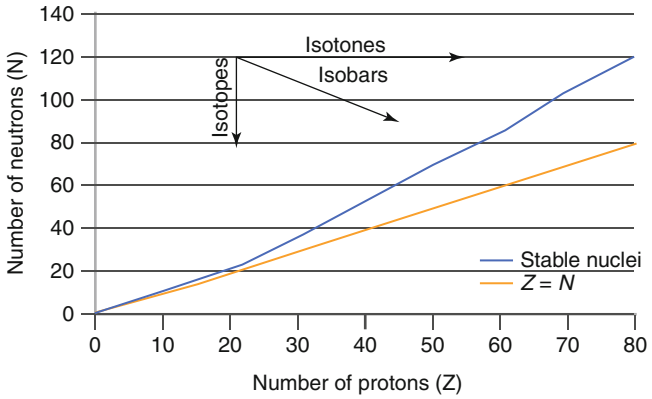

Figure 1-1. Stability of the nucleus. This graph plots as a *blue line*, the number of neutrons versus the number of protons for stable nuclei. The *yellow line* indicates a neutron–proton ratio of 1. Only nuclides with low proton numbers fall on this line. For the *blue line*, note that as the number of protons increases, more neutrons are required to keep the nucleus stable. Nuclides with neutron–proton ratios that are not on the *blue line* of stable nuclei are unstable and, thus, radioactive. These radioactive nuclides are known as *radionuclides*. The type of radioactivity emitted depends on which side of the line the radionuclide is found. Isotopes are a family of nuclides that all have the same number of protons, or atomic number (Z), and are not necessarily radioactive. Isotones are nuclides with the same number of neutrons (*N*), and isobars have the same mass number (*A*) or number of mass particles in the nucleus ($A = Z + N$).

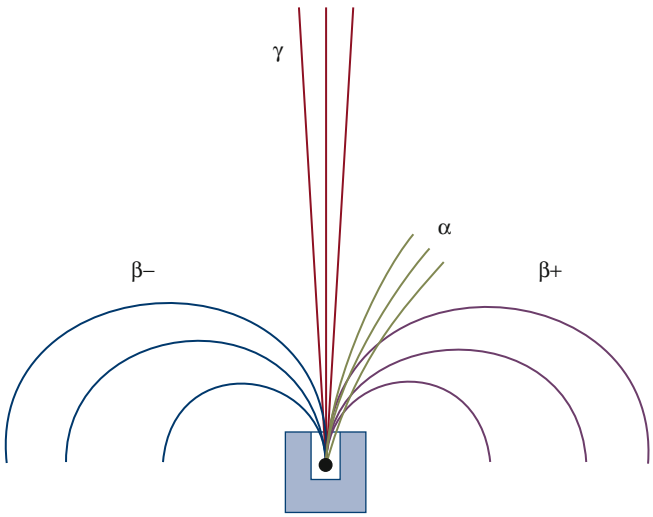

Figure 1-2. Types of radiation. This diagram represents the path deviation of different types of radiation from nuclei by a magnetic field perpendicular to the page. The direction of the deflection depends on the charge of the radioactive particle. The least penetrating radiation is deflected to the right and corresponds to the heaviest radiation, called an alpha particle (α). An α particle is actually the nuclei of a helium atom (two protons plus two neutrons) with a positive charge. The moderately penetrating radiation deflected in the direction opposite to an α particle consists of negative particles called beta particles (β). Because these particles are more strongly bent, they are lighter than the α particles. The β particles are actually electrons emitted from the nucleus. Showing the same degree of penetration but bending in the direction opposite to the β particles are positron particles, or positive electrons (β+). These particles are made of antimatter and emitted by positron tracers. The radioactive particles that go straight and are not deflected do not consist of charged particles. They are called gamma (γ)-rays and have been shown to be identical to particles emitted from an x-ray tube [1]. Both x- and γ-rays are called photons and are used in nuclear cardiology imaging.

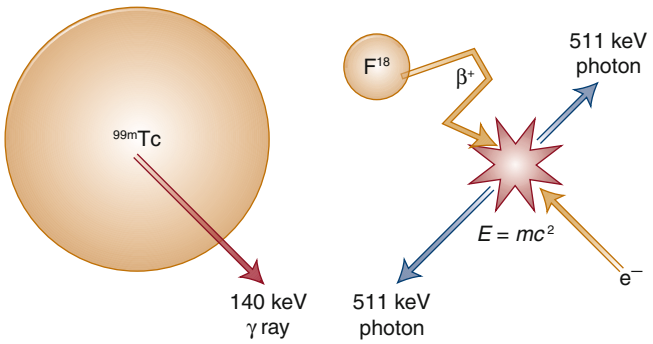

FIGURE 1-3. Single-photon emission CT (*SPECT*) versus positron emission tomography (PET) radionuclides. This figure shows two very different types of radionuclides, technetium-99m (^{99m}Tc) and fluorine-18 (^{18}F). ^{99m}Tc is a large radionuclide that emits a single photon or γ-ray per radioactive decay that is used in SPECT to create images. The energy of the emitted photon is 140 keV. The *m* in ^{99m}Tc means that the nucleus is metastable (almost stable but really unstable). ^{18}F is a much smaller radionuclide that emits a positron (β+) antiparticle. This ionized antiparticle travels through a medium interacting with it, losing energy and slowing down until it interacts with an electron, usually from some atom. Because the electron and the positron are antiparticles of each other (i.e., same mass but opposite charge), they undergo a phenomenon called *pair annihilation*. In pair annihilation, the mass of both particles disintegrates and is converted into energy as explained by Einstein's famous equation, $E=mc^2$, where *E* is the emitted energy, *m* is the mass of the two particles, and *c* is the speed of light in a vacuum. Due to the nature of the interaction, the energy is usually emitted in the form of two photons traveling in exactly opposite directions from each other and each having the same energy, 511 keV, which is the energy equivalent to the rest mass of an electron. These two photons are used to create images in PET.

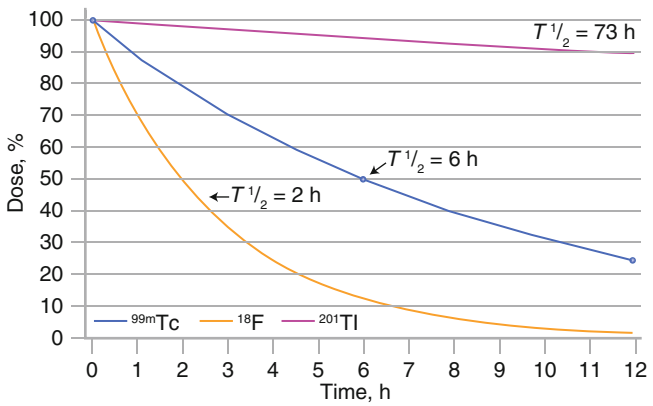

FIGURE 1-4. Radioactive decay law: concept of half-life. This diagram shows decay curves for three different radionuclides: technetium-99m (^{99m}Tc), fluorine-18 (^{18}F), and thallium-201 (^{201}Tl). The decay curves express the amount of radioactive nuclides that have not decayed as a function of time. The shorter the interval between emissions for a specific radionuclide, the faster the radioactivity is depleted. It is practical to express the rate of radioactive transformations (disintegrations) by specifying the period during which half of all the atoms initially present will disintegrate. This period of time is known as the *half-life*, or *T*½. Note from the graph that the ^{18}F curve is disintegrating the fastest of the three radionuclides and that it reaches a level of 50 % of original at 2 h; therefore, the half-life of ^{18}F is 2 h. Compare this with the half-life of ^{201}Tl, which is 73 h, and the half-life of ^{99m}Tc, which is 6 h. The amount of radioactive nuclide is specified in terms of its disintegration rate or its activity. This relationship is provided by the radioactive decay law:

$$A(t) = A_0 e^{-(0.693t)} / T\frac{1}{2}.$$

In this equation, *A(t)* is the radioactivity remaining at time *t*, A_0 is the activity at time 0, and *T*½ is the half-life of the radionuclide.

A common unit of radioactivity is the curie (Ci), which is 3.7×10^{10} disintegrations/s. Another common unit of radioactivity used is the becquerel (Bq), which is one disintegration per second. One thousandth of a curie is a millicurie (mCi), which corresponds to 3.7×10^7 disintegrations per second. Note from the graph that if a 40-mCi dose of a ^{99m}Tc radiopharmaceutical (radioactive pharmaceutical) is delivered to an imaging clinic at 6 a.m., 6 h later, at noon, only half—or 20 mCi—remains, and at 6 p.m., only half of that—or 10 mCi—remains.

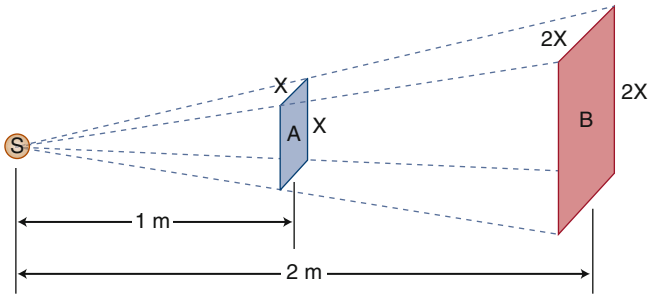

Figure 1-5. Inverse square law. This diagram illustrates the concept of the inverse square law for radioactivity. The intensity of a radioactive point source at a distance from the source obeys the same law as for visible light. If the amount of radioactivity at the point source (*S*) remains constant, then the intensity of the radioactivity (number of photons) passing through a flat surface is inversely proportional to the square of the distance from the source. At a distance of 1 m, the diverging radioactive beam covers an area (*A*, *small square*) with each side of dimension x, or an area of x^2. At 2 m, the diverging beam covers an area (*B*, *large square*) in which each side is now twice as long as *A* (2x) and the area is $4x^2$, which is four times the area at 1 m. Because the amount of radioactivity remains constant, the number of photons falling on *square A* must spread out over four times as large an area by the time it reaches *square B*. Thus, the activity per unit area at *B*, which is twice as far as *A* from the source, is one fourth of the activity passing through *A* [2]. The value of this principle to radiation workers is that they can significantly reduce their radiation burden just by increasing their distance between themselves and a radioactive source, such as a patient already injected with a radioactive dose.

Figure 1-6. Interaction of radiation with matter: photons. High-energy photons, such as γ- and x-rays, interact with matter in three ways that are relevant to nuclear medicine: through the photoelectric effect, Compton scattering, and pair production [3]. Each of these processes results in the emission of charged particles (electrons or positrons) that produce much more ionization than the original event. Thus, high-energy photons are classified as secondary ionizing radiation.

(**a**) The photoelectric effect (or photoelectric absorption) occurs when a photon (γ- or x-ray) is completely absorbed as it interacts with an inner-shell electron. All the energy is lost to the electron, now called a photoelectron, which is emitted from the atom with an energy equivalent to the photon energy (E_0) less the binding energy of the electron ($E_{Binding}$). After photoelectric absorption, the atom has a vacancy in an inner electron shell that will be filled by an outer-shell electron, resulting in the emission of characteristic x-rays and possibly auger electrons.

Compton scattering occurs when a photon interacts with an outer-shell electron, changing its direction and losing some energy. The amount of energy of the photon after scattering depends on the angle of scatter (q) according to the following formula:

$$E_{sc} = E_0 / 1 + \left(E_0 / 511\text{keV}\right) \times \left(1 - \cos\left(\theta\right)\right).$$

In this formula, E_0 is the energy of the photon before scattering, E_{sc} is the energy of the photon after scattering, and θ is the angle between the photon's original path and its new one. The larger the angle, the more energy is lost. Maximum energy is lost when the photon reverses course (θ=180°) and backscatters. All the energy lost to the γ-ray ($E_0 - E_{sc}$) is transferred to the electron, which on ejection from the atom is called a recoil electron (the binding energy of the outer-shell electron is negligible). Energies of Compton-scattered photons as a function of angle are given in Table 1.1.

Pair production occurs when a photon passes near a charged particle (usually the nucleus of an atom). The photon is destroyed and a positron–electron pair (β+, β–) is created. According to the formula $E=mc^2$, the mass of the electron is equivalent to 511 keV; thus, the photon has to have at least 1,022 keV for pair production to occur. Energy in excess of 1,022 keV is shared by the positron and the electron as kinetic energy. Due to the high energy required for the process, it is of little importance in clinical nuclear medicine laboratories.

(**b**) The most probable interactions between high-energy photons and matter depend on the energy of the photons and the density of the material. Compton scattering is by far the most common interaction within the patient from the photons produced by clinical radiopharmaceuticals. The photoelectric effect is more likely to take place in the lead shielding of the collimator.

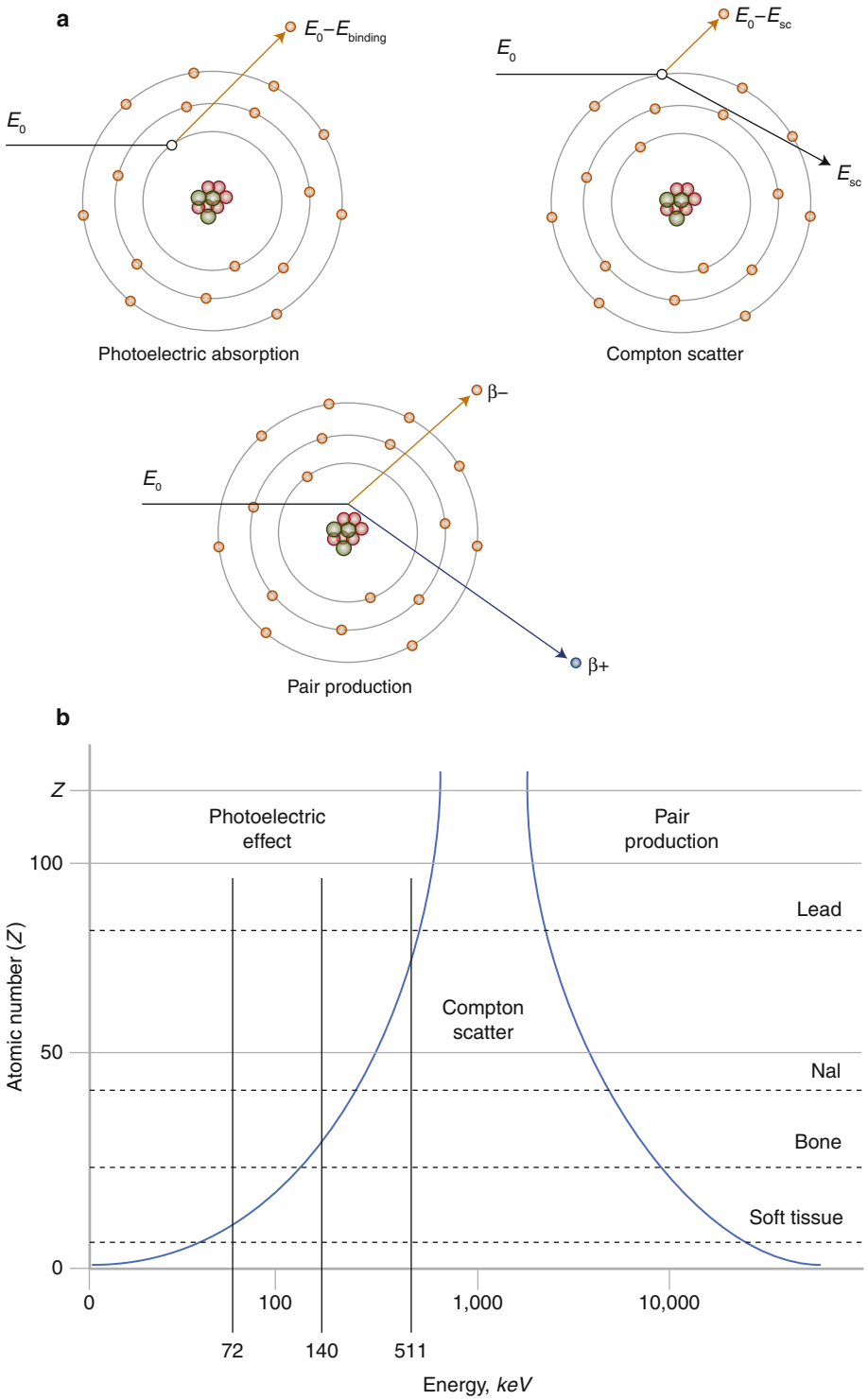
a
E_0
$E_0 - E_{binding}$
Photoelectric absorption
E_0
$E_0 - E_{sc}$
E_{sc}
Compton scatter
E_0
β–
β+
Pair production
b
Z
100
50
0
Atomic number (Z)
Photoelectric effect
Pair production
Compton scatter
Lead
NaI
Bone
Soft tissue
0
100
1,000
10,000
72
140
511
Energy, keV

Energies of compton-scattered photons (E_0) in kiloelectron volts					
Scattering angle					
Radionuclide	E_0, keV	30°	60°	90°	180°
Thallium-201	72	71	67	63	56
Technetium-99m	140	135	123	110	90
Positron annihilation	511	451	341	256	170

Table 1-1. Energies of Compton-scattered photons (E_0) in kiloelectron volts. This table shows the relationship between the photopeak energy of common radionuclides used in nuclear cardiology, the scattering angle of the Compton-scattered photon, and the resulting energy of that photon. Note that in many instances, the original emitted photon may undergo a large scatter angle and still be counted by a 20 % energy window in a camera's pulse height analyzer.

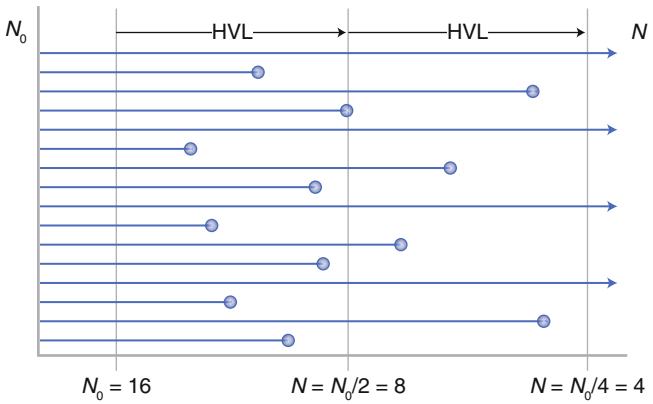

Figure 1-7. Photon attenuation. As photons are absorbed through the photoelectric effect or scattered away from the detector through Compton scattering, their loss is called *attenuation*. The percentage of photons lost depends on the energy of the photons, the density of the material, and the material's thickness. The dependence on thickness is straightforward: the thicker the material, the more photons will be absorbed. The thickness at which half of the photons are absorbed is called the *half-value layer* (HVL). In the example, N0 photons pass through a material after 1 HVL, one half of photons, has been lost; after 2 HVLs, only one fourth of the photons is left. In practice, the attenuation of a beam of photons is usually calculated using the linear attenuation coefficient (μ=ln2/HVL) in the following equation:

$$I = I_0 e - \mu^x.$$

In this equation, I_0 is the initial beam intensity and I is the intensity after traveling through thickness x. The values of linear attenuation coefficients depend on the energy of the photon and the composition of the material. The denser the material and the higher the energy of the photon, the less attenuation and the lower the value of m. Linear attenuation coefficients and HVLs for radionuclides and materials of interest to nuclear cardiology are given in Table 1.2.

Linear attenuation coefficients and half-value layers							
		Soft tissue (1.0 g/cm³)		Bone (1.9 g/cm³)		Lead (11.3 g/cm³)	
Radionuclide	**Energy, keV**	**μ, 1/cm**	**HVL, cm**	**μ, 1/cm**	**HVL, cm**	**μ, 1/cm**	**HVL, cm**
Thallium-201	72	0.191	3.62	0.493	1.40	39.1	0.018
Technetium-99m	140	0.153	4.52	0.295	2.35	30.7	0.023

Table 1-2. Linear attenuation coefficients and half-value layers (HVL). This table shows the relationship between the photopeak energy of common radionuclides used in nuclear cardiology and their corresponding linear attenuation coefficient (μ) and HVL in soft tissue, bone, and lead. Note that the denser the material, the smaller the HVL has to be in order to reduce the photon beam by 50 %. The values in the table were calculated from data obtained from Hubble and Seltzer [4]

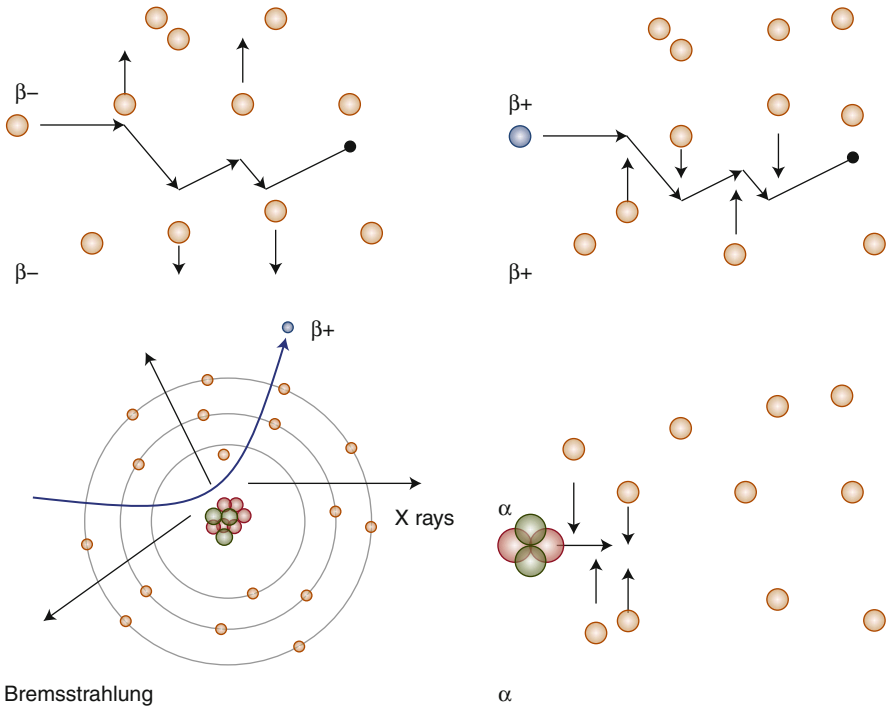

Figure 1-8. Interaction of radiation with matter: charged particles. High-energy charged particles such as alpha particles (α), beta particles (β), and the photoelectrons and recoil electrons discussed earlier slow down and lose energy as they pass through matter. This loss is a result of the forces their charges exert on the electrons (and, to a lesser extent, on the nuclei) of the material. These interactions are called *collisions*. The loss of energy is termed *collisional losses* (even though it does not actually involve a collision between the two particles) or *radiation losses*, depending on the nature of the encounter.

The β particles have the same mass as electrons, and as they pass through material, the electrical forces of the electrons (attractive for β+ and repulsive for β−) cause them to change course with each interaction. These collisions transfer some of the b particles' energy to the orbital electrons, causing them to escape their orbit (the ejected electron is called a delta ray [Δ]) or to be raised to a higher energy state (excitation). Due to their tortuous path, the depth at which β particles will penetrate a material (range) varies between different β particles of the same energy, a process called straggling. Two measures of the depth of penetration of beta particles are the extrapolated range (an estimation of the maximum positron penetration) and the average range (the mean penetration). A short positron range is desirable for positron emission tomography (PET) imaging because PET determines the origin of the electron–positron annihilation event, not the actual site of the positron emission. Table 1.3 presents extrapolated and average ranges for several PET radionuclides.

The α particles are much more massive than electrons. As collisions occur between α particles and electrons, the electrons are excited or swept from orbit, but the encounter has little effect on the direction of the α particle. As a result, α particles of the same energy all have the same range, with very little straggling. The range is also very small, so that α particles present very little danger as an external radiation source given that they are stopped by a few centimeters of air or a few micrometers of tissue.

Positron particle range

		Extrapolated range, cm		Average range, cm
Radionuclide	**Maximum energy, MeV**	**Air**	**Water**	**Water**
Carbon-11	0.961	302	0.39	0.103
Nitrogen-13	1.19	395	0.51	0.132
Oxygen-15	1.723	617	0.80	0.201
Fluoride-18	0.635	176	0.23	0.064
Rubidium-82	3.35	1,280	1.65	0.429

Data from Cherry et al. [5]

Table 1-3. Positron particle range. This table shows the relationship between the maximum energy of the emitted positron and the distance range that these particles travel in air and water. Note that the lower the energy and the denser the medium, the less it travels and, thus, the higher the resulting spatial resolution.

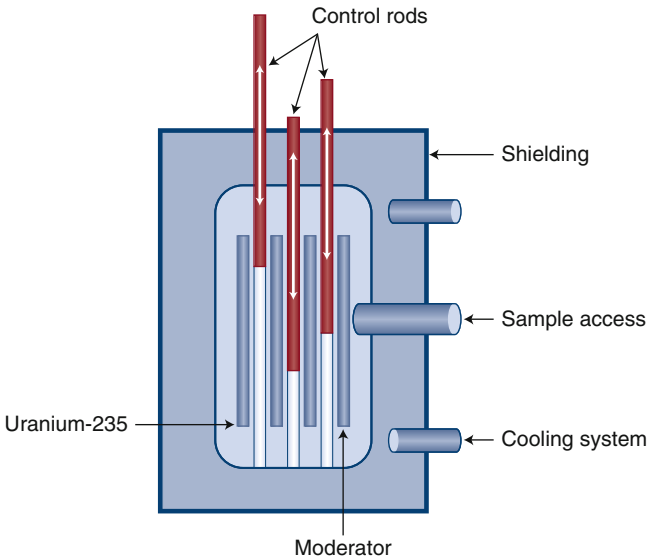

Figure 1-9. Formation of radionuclides: nuclear reactors. The radionuclides used in nuclear cardiology do not occur naturally and must be manufactured. This may be done by extracting them from the spent fuel of a nuclear reactor, bombarding a target nuclide with high-energy neutrons to make a nuclide that is neutron rich (too many neutrons to be stable), or bombarding a target with high-energy positively charged particles, such as protons, using a cyclotron or other particle accelerator to make proton-rich nuclides. Generators are devices that allow the separation of a daughter radionuclide from the parent in a shielded container that may be transported long distances from the manufacturing site (reactor or accelerator).

Nuclear reactors are an important source of radionuclides for nuclear medicine, including iodine-131 and xenon-133. Most importantly, molybdenum-99 (^{99}Mo), the parent of technetium-99m, is produced in a nuclear reactor. The heart of a nuclear reactor is a core of fissionable material (usually uranium-235 [^{235}U] and ^{238}U). Fission splits the uranium nucleus into two lighter nuclei and produces two or three fission neutrons. Some of these neutrons strike other uranium nuclei, converting them to ^{236}U. ^{236}U quickly undergoes fission and produces many more fission neutrons, which stimulate even more fission events. The uranium in the core is surrounded by a moderator ("heavy water" and graphite) that slows down the fission neutrons to an energy that is more likely to produce further reactions. The ensuing nuclear chain reaction is regulated by control rods that absorb neutrons made of boron or cadmium. Fission products usually have an excess of neutrons and decay further with emission. More than 100 nuclides are created in the fission process. These fragments can be extracted by chemical means from material removed from the core. Another way to use a nuclear reactor to produce radionuclides, neutron activation, is to place a target into the high-neutron flux of the core while keeping it isolated from the core itself. ^{99}Mo can be produced by either process but most is extracted as a fission fragment.

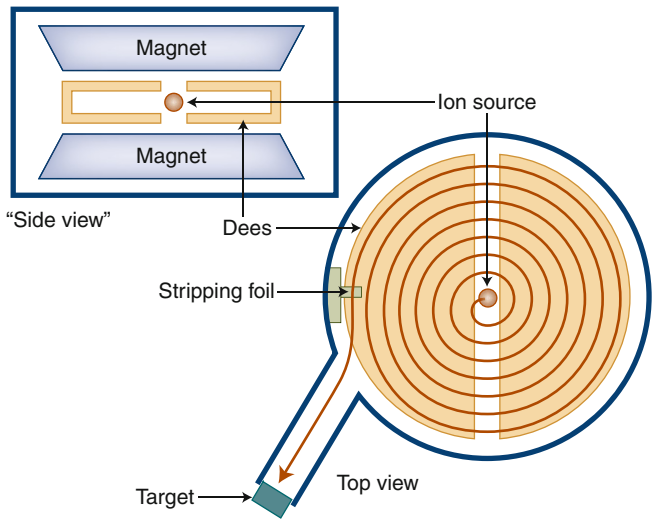

Figure 1-10. Formation of radionuclides: cyclotrons. Cyclotrons are charged particle accelerators that are used to produce radionuclides by bombarding a target with particles or ions that have been accelerated to high rates of speed. The two basic components of a cyclotron are a large electromagnet and semicircular, hollow electrodes called "dees" because of their shape. Ions are injected into the center of the device between the dees. An alternating current applied to the dees causes the ions to be attracted to one side. Once inside the dee, the ion will travel in a curve because any charged particle moving in a magnetic field (supplied by the electromagnet) moves in a circular path. Although there is no electric field inside the dee, the current is carefully timed so that the polarization of the dees changes as the particles emerge from one side. This accelerates the ions, and their arc of travel becomes larger as they move faster and faster, picking up speed each time they cross the gap between the dees. At the maximum radius, the ions are deflected out of the cyclotron and strike a target, creating new nuclides. An example of this is the use of a cyclotron to bombard an oxygen-18 target with protons, resulting in conversion of the nucleus to fluorine-18 (after the emission of a neutron). Several cyclotron-produced radionuclides used in nuclear cardiology are listed in Table 1.4.

Positive-ion cyclotrons accelerate α particles or protons and use an electrostatic deflector to direct the ion beam to the target. Negative-ion cyclotrons, as shown in this figure, accelerate negative hydrogen (H^-) ions, a proton with two electrons. A stripping foil, made of carbon, strips off the two electrons from the ion, leaving a proton. The positive charge of the proton causes it to arch in the opposite direction, which in turn causes the beam to exit the cyclotron and strike the target. Most hospital- and community-based cyclotrons are negative-ion cyclotrons because they require less shielding and are more compact than positive-ion cyclotrons.

A. Common SPECT radionuclides for use in nuclear cardiology

Radionuclide	Production	Decay	Emission, keV	Half-life, h
Iodine-123	Cyclotron	Electron capture	159 (γ-ray)	13.21
Thallium-201	Cyclotron	Electron capture	68–80 x-ray; 167 (10 %; γ-ray)	73
Technetium-99m	Generator	Internal transition	140 (γ-ray)	6

B. Common PET radionuclides for use in nuclear cardiology

Radionuclide	Production	Positron energy, keV	Half-life, h
Oxygen-15	Cyclotron	735	122 s
Nitrogen-13	Cyclotron	491	9.96 min
Carbon-11	Cyclotron	385	20.3 min
Fluoride-18	Cyclotron	248	110 min
Rubidium-82	Generator	1,523	1.3 min

Table 1-4. Common radionuclides for use in nuclear cardiology. These tables compare the energy of the radiation, half-lives, and modes of production of single-photon emission CT (SPECT; **A**) versus positron emission tomography (PET) radionuclides (**B**) commonly used in nuclear cardiology procedures. Note that due to the short half-life of most cyclotron-produced PET tracers, a cyclotron must be located nearby. Only fluorine-18 is routinely distributed commercially [6].

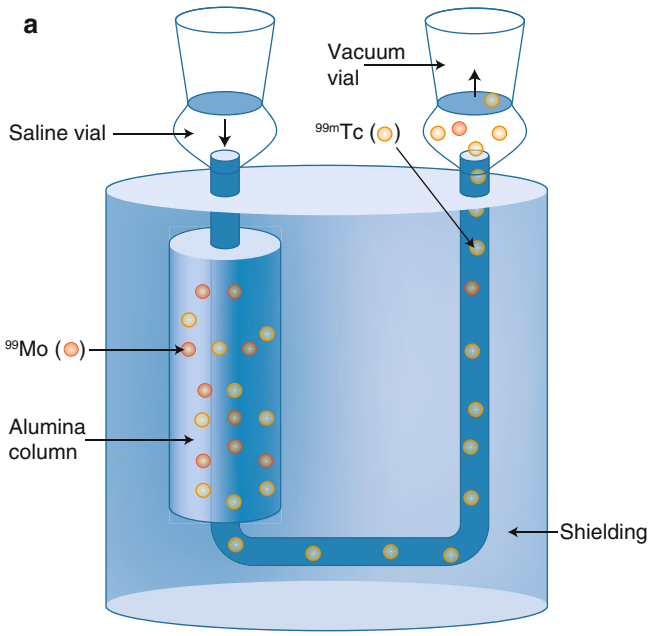
a
Vacuum vial
Saline vial
99mTc ( )
99Mo ( )
Alumina column
Shielding

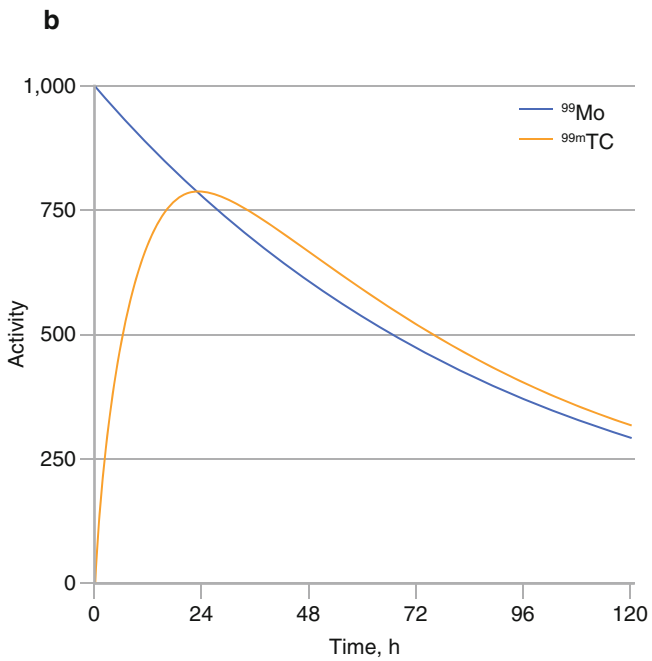
b
1,000
750
500
250
0
Activity
99Mo
99mTC
0
24
48
72
96
120
Time, h

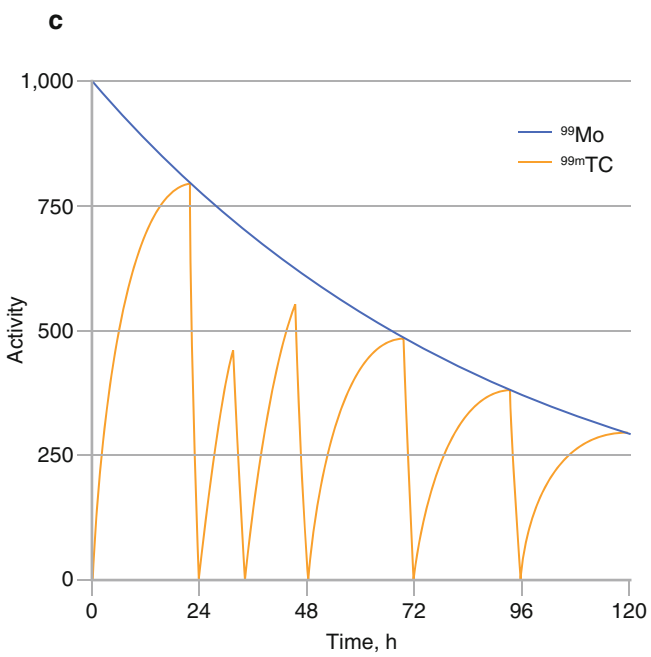
c
1,000
750
500
250
0
Activity
99Mo
99mTC
0
24
48
72
96
120
Time, h

FIGURE 1-11. Formation of radionuclides: molybdenum-99–technetium-99m (^{99}Mo–^{99m}Tc) generator. Generators are devices that allow the separation of a radionuclide from a relatively long-lived parent, allowing the production of short-lived radionuclides at a location remote from a reactor or cyclotron (such as a hospital, clinic, or local radiopharmacy). The daughter is continuously replenished by the parent inside the generator, which shields both radionuclides while allowing the daughter to be extracted repeatedly [7].

(**a**) The most common generator used in nuclear medicine is the ^{99}Mo-^{99m}Tc generator, which produces ^{99m}Tc (half-life [$t½$], 6 h) from the β decay of ^{99}Mo ($t½$, 66 h). The ^{99}Mo is produced in a nuclear reactor. The heart of the generator is an alumina column impregnated with ^{99}Mo. A vacuum vial is used to pull saline out of a second vial through the porous column. Technetium (both ^{99m}Tc and ^{99}Tc) is washed out of the column by the saline and is collected in a vacuum vial, leaving the ^{99}Mo behind. The generator must be well shielded because ^{99}Mo emits both β particles and 740–780–keV γ-rays. The process of extracting ^{99m}Tc from the generator is called *milking* or *elution*, and the extracted ^{99}Tc-saline solution is called eluate. After milking, the ^{99m}Tc solution must be tested for ^{99}Mo and aluminum. ^{99}Mo is detected by using a dose calibrator and a shield that blocks the low-energy photon from 99mTc. The maximum amount of ^{99}Mo allowed under Nuclear Regulatory Commission regulations is 0.15 Bq ^{99}Mo per kilobecquerel (kBq) ^{99m}Tc (0.15 Ci ^{99}Mo per millicurie ^{99m}Tc). Aluminum is detected chemically, with a maximum permissible level of 10 μg/mL of eluate. (**b**) The ^{99m}Tc is produced by the β decay of ^{99}Mo in the alumina column if the generator is undisturbed. This process is an example of transient equilibrium, in which the parent's half-life is somewhat longer than the daughter's half-life. After a few hours, the daughter activity is almost equal (actually slightly higher) to the parent activity. (**c**) Activity in the generator with repeated milkings is shown. Fortunately, the optimal frequency for milking the generator is at intervals slightly less than 24 h. The dip at 32 h shows that if the generator is milked, the process of ^{99m}Tc buildup begins again (and, in this case, results in only slightly less activity at the next regular milking). ^{99}Mo-^{99m}Tc generators are designed to last at least 2 weeks in the nuclear pharmacy.

Another generator of importance to nuclear cardiology is the strontium-82 (^{82}Sr)–rubidium-82 (^{82}Rb) generator. ^{82}Rb ($t½ = 1.3$ min) is produced by a β decay of ^{82}Sr ($t½ = 25$ day, manufactured using an accelerator). The daughter activity equals the parent activity very soon after elution and allows elution every hour. This is an example of secular equilibrium in which the parent's half-life is a great deal longer than the daughter's half-life. The short half-life of ^{82}Rb makes it impractical to transport the dose to the patient. The generator is designed to deliver the dose directly into an intravenous line. ^{82}Rb generators are designed to last about 1 month in the clinic. ^{82}Sr and ^{85}Sr may be low-level contaminants and are found in routine quality control by assaying the eluent after complete decay of the ^{82}Rb.

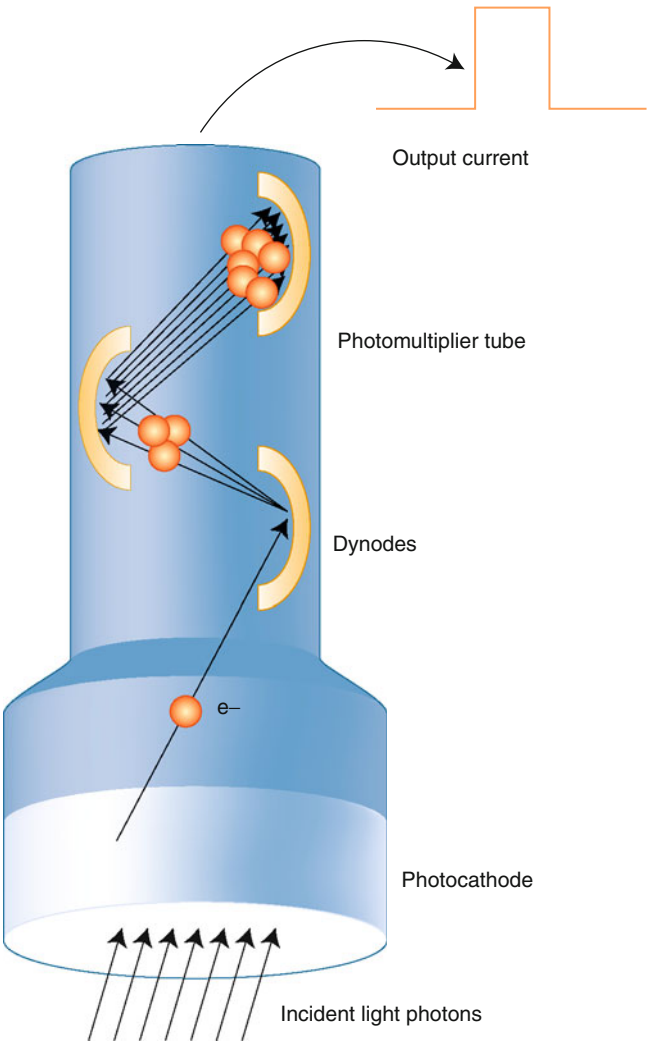

Figure 1-12. Operation of photomultiplier tubes (*PMTs*). PMTs convert energy from visible light into an electric signal. Light interacting with the material in the photocathode causes it to release electrons, which are accelerated along the tube by a high-voltage differential. As the electrons travel through the tube, they strike metal electrodes called dynodes, at which point even more electrons are ejected. This cascade of multiplication continues until the electrons are output as a current at the other end. The voltage (height) of the pulse generated by the PMT is directly proportional to the amount of visible light that strikes the photocathode.